Fermandjian, S., Tran-Dinh, S., Savrda, J., & Sala, E. (1975) *Biochim. Biophys. Acta 399*, 313.
Fischer, G., Heins, J., & Barth, A. (1983) *Biochim. Biophys. Acta 742*, 452.
Galardy, R. E., & Liakopoulou-Kyriakides, M. (1982) *Int. J. Pept. Protein Res. 20*, 144.
Grathwohl, C., & Wüthrich, K. (1976) *Biopolymers 15*, 2025.
Grathwohl, C., & Wüthrich, K. (1981) *Biopolymers 20*, 2623.
Liakopoulou-Kyriakides, M., & Galardy, R. E. (1979) *Biochemistry 18*, 1952.
Lin, L.-N., & Brandts, J. F. (1979a) *Biochemistry 18*, 43.
Lin, L.-N., & Brandts, J. F. (1979b) *Biochemistry 18*, 5017.
Lin, L.-N., & Brandts, J. F. (1980) *Biochemistry 19*, 3055.
Lin, L.-N., & Brandts, J. F. (1983a) *Biochemistry 22*, 553.
Lin, L.-N., & Brandts, J. F. (1983b) *Biochemistry 22*, 559.
Lin, L.-N., & Brandts, J. F. (1983c) *Biochemistry 22*, 564.
Lin, L.-N., & Brandts, J. F. (1983d) *Biochemistry 22*, 573.
Toma, F., Lam-Thanh, H., Piriou, F., Heindl, M.-C., Lintner, K., & Fermandjian, S. (1980) *Biopolymers 19*, 781.
Yoshimoto, T., & Tsuru, D. (1978) *Agric. Biol. Chem. 42*, 2417.
Yoshimoto, T., Ogita, K., Walter, R., Koida, M., & Tsuru, D. (1979) *Biochim. Biophys. Acta 569*, 184.
Yoshimoto, T., Walter, R., & Tsuru, D. (1980) *J. Biol. Chem. 255*, 4786.

Acyl Carrier Protein from *Escherichia coli* I. Aspects of the Solution Structure As Evidenced by Proton Nuclear Overhauser Experiments at 500 MHz†

K. H. Mayo, P. M. Tyrell, and J. H. Prestegard*

ABSTRACT: The downfield aromatic (6–8 ppm) and upfield ring current shifted methyl regions (1–0 ppm) in the proton nuclear magnetic resonance spectrum of acyl carrier protein (ACP) from *Escherichia coli* have been examined at 500 MHz by using nuclear Overhauser methods. The data are analyzed in terms of the secondary structural model of Rock & Cronan (1979) [Rock, C. O., & Cronan, J. E., Jr. (1979) *J. Biol. Chem. 254*, 9778–9785], which suggests the existence of four α-helical segments joined by three β-turns, and a short coil at the C terminus of the protein. Nuclear Overhauser effects among Tyr-71, Ile-69, Ile-72, and His-75 allow refinement of the secondary structure of the C terminus. Nuclear Overhauser effects among Tyr-71, Phe-28, and three Ile's also place stringent limitations on the folding of the four α-helices. These data allow the proposal of a tertiary structural model for ACP.

Acyl carrier proteins (ACPs)[1] are known to play a key metabolic role in the synthesis of fatty acids in both prokaryotic and eukaryotic organisms (Thompson, 1981). Although the mode of association within the fatty acid synthetase system may vary depending on a particular organism's position on the evolutionary ladder, all known ACPs share the capacity to carry a growing fatty acid chain bound through a thio ester linkage to a 4′-phosphopantetheine prosthetic group, phosphodiester linked to a serine of ACP (Thompson, 1981). ACPs interact with at least 12 different enzymes involved in fatty acid synthesis and utilization. The diversity in this set of interactions and the suggestion that structural properties of ACPs may control relative enzymatic activities among members of this set (Schultz et al., 1969) have stimulated much interest in the structural characterization of ACP.

Among all known ACPs, ACP from *Escherichia coli* is perhaps the best characterized (Prescott & Vagelos, 1972; Vanaman et al., 1968a,b). A small protein of 8847 daltons, ACP from *E. coli* contains 77 amino acid residues, a large proportion being acidic (~29%) and a small proportion (~8%), clustered at the NH terminus, being positively charged. Although the sequence of ACP has been known for some time (Vanaman et al., 1968a,b), efforts to crystallize it have failed; therefore, no X-ray crystal structure exists. From an interpretation of optical rotary dispersion (Takagi & Tanford, 1968; Prescott et al., 1969) and circular dichroism studies (Schultz, 1975), ACP seems to possess a high α-helix content. More recently, Rock & Cronan (1979) have applied the predictive algorithm of Chou & Fasman (1974a,b, 1978a,b) to ACP; α-helical regions are predicted to exist between residues 3–21, 26–32, 37–53, and 58–69, with β-turns interrupting the α-helical segments, yielding a rough, first approximation to the secondary structure.

In the present study, the objective is to test and refine the proposed secondary structure and gain some insight into the tertiary structure or folding of the ACP molecule. High-resolution ^{1}H NMR (500 MHz) methods, analogous to those applied to small soluble proteins by other authors over the past few years (Gordon & Wüthrich, 1978; Poulsen et al., 1980; Wagner & Wüthrich, 1979; Dobson et al., 1980), have been employed. We present, here, results based largely on cross-relaxation rate measurements (NOEs) on reduced acyl carrier protein (ACP-SH) from *E. coli* B cells. Under suitable conditions, measured cross-relaxation rates can be interpreted in terms of interresidue (proton) distances and the general characteristics of the predictive model of Chou and Fasman

† From the Department of Chemistry, Yale University, New Haven, Connecticut 06511. *Received May 3, 1983.* This work was supported by a grant from the National Science Foundation (PCM-7821101) and benefited from NMR facilities made available through Grant CHE-7916210 from the National Science Foundation.

[1] Abbreviations: ACP, acyl carrier protein; ACP-SH, reduced acyl carrier protein; DSS, sodium 4,4-dimethyl-4-silapentanesulfonate; NOE, nuclear Overhauser effect; FID, free induction decay.

0006-2960/83/0422-4485$01.50/0

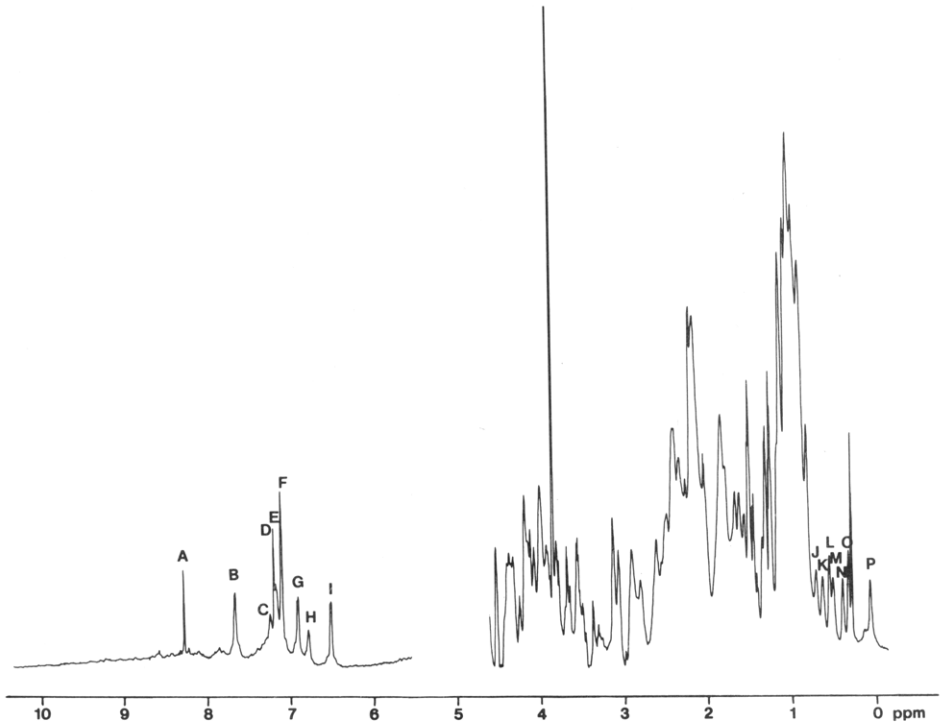

FIGURE 1: NMR spectrum at 500 MHz of ACP-SH. The spectrum represents 512 accumulations over a period of ~12 min using a 90° pulse on a 0.5-mL sample at concentrations of 3 mM ACP-SH in 30 mM $MgSO_4$, pH 5.7 at 303 K. The large, central HDO resonance has been omitted for clarity.

(Rock & Cronan, 1979) for ACP tested. Such through-space interaction (NOE) data have the potential to yield some strong structural information regarding the tertiary as well as the secondary structure of ACP-SH.

Materials and Methods

Native acyl carrier protein (ACP) was purified from *Escherichia coli* B cells (Grain Processing) by using the method of Rock & Cronan (1980) and reduced to free sulfhydryl by the method of Cronan & Klages (1981). Purity was checked by proton NMR, amino acid analysis, and native acrylamide gel electrophoresis (Ray & Cronan, 1976). Ellman's test for sulfhydryl reactivity (Ellman, 1959) verified the existence of an active, free sulfhydryl on the prosthetic group.

Samples for ^1H NMR measurements were passed through a Chelex column, dialyzed against deionized/distilled H_2O, freeze-dried, and redissolved in D_2O immediately before the experiment. The final protein concentration was about 3 mM in approximately 30 mM magnesium sulfate.

^1H NMR spectra were recorded in the Fourier mode on a Bruker WM-500 spectrometer at 303 or 288 K. The solvent deuterium signal was used as the field-frequency lock. All chemical shifts are quoted in parts per million (ppm) downfield from sodium 4,4-dimethyl-4-silapentanesulfonate (DSS). NOEs were generated by irradiating the desired peak for times of 0.1, 0.2, and 0.4 s at a power level sufficient to null z magnetization of the irradiated peak in 0.05 s. A 2-ms delay was introduced before accumulation to reduce transient effects, and a time of 1.5 s was allowed between accumulations (accumulation time of 1.48 s) to allow for recovery of z magnetization. Difference spectra were obtained by subtracting the free induction decay (FID) of the irradiated peak spectrum from the FID of a control spectrum which had been irradiated in a region where no resonances occur under the same experimental conditions. NOEs were determined by dividing areas of peaks in the difference spectrum by the area of the irradiated peak and correcting for differences in the number of protons.

Results

Assignments. Figure 1 shows a proton NMR spectrum (500 MHz) of reduced acyl carrier protein (ACP-SH) in D_2O at pH 5.7 and in 30 mM $MgSO_4$. The clearly resolved (resolution-enhanced) downfield region of the spectrum (Figure 2) consists of resonances from the aromatic amino acids Phe-28, Phe-50, Tyr-71, and His-75. Galley et al. (1978) had previously assigned resonances at 8.27 (A) and 7.19 ppm (D) to the C(2)H and C(4)H protons of His-75, as well as the two (two-proton) resonances at 6.89 (G) and 6.49 ppm (I) to the 2,6 and 3,5 protons of Tyr-71, respectively. At 500 MHz, one can clearly resolve the singlet C(4) proton of His-75 from a triplet of intensity 1 at 7.23 ppm (C) and a triplet of intensity 2 at 7.17 ppm (E). Spin-decoupling experiments show the triplet of intensity 2 at 7.17 ppm (E) to be scalar coupled to the doublet of intensity 2 at 7.65 ppm (B) and the triplet of intensity 1 at 7.23 ppm (C). These three groups of resonances, therefore, belong to a single phenylalanine—denoted phenylalanine-I—and must represent its 4, 2,6, and 3,5 protons. The remaining triplet of intensity 1 at 6.78 ppm (H) must belong to the 4 proton of the remaining phenylalanine, Phe-II, and the set of resonances of intensity 4 at 7.08 ppm (F) must belong to the 2,6 and 3,5 protons of phenylalanine-II.

The upfield part of the spectrum is less well resolved. Some exceptions are high field shifted resonances of intensity 3 at 0.66 (J), 0.60 (K), 0.53 (L), 0.50 (M), 0.41 (N), 0.34 (O), and 0.12 (P) ppm. These peaks are candidates for resonances from methyl groups on residues which are proximal to aromatic residues, thereby being ring current shifted to their high-field positions. Other resonances in this high-field region vary in intenstiy from sample to sample and are associated with impurities in the buffer. Resolution enhancement (Figure 3) shows resonances at 0.66 (J), 0.60 (K), and 0.50 (M) ppm to be triplets and resonances at 0.53 (L), 0.41 (N), 0.34 (O), and 0.12 (P) ppm to be doublets. The triplets are assignable to isoleucines since only isoleucine has a methyl group spin coupled to two other vicinal protons. There are seven iso-

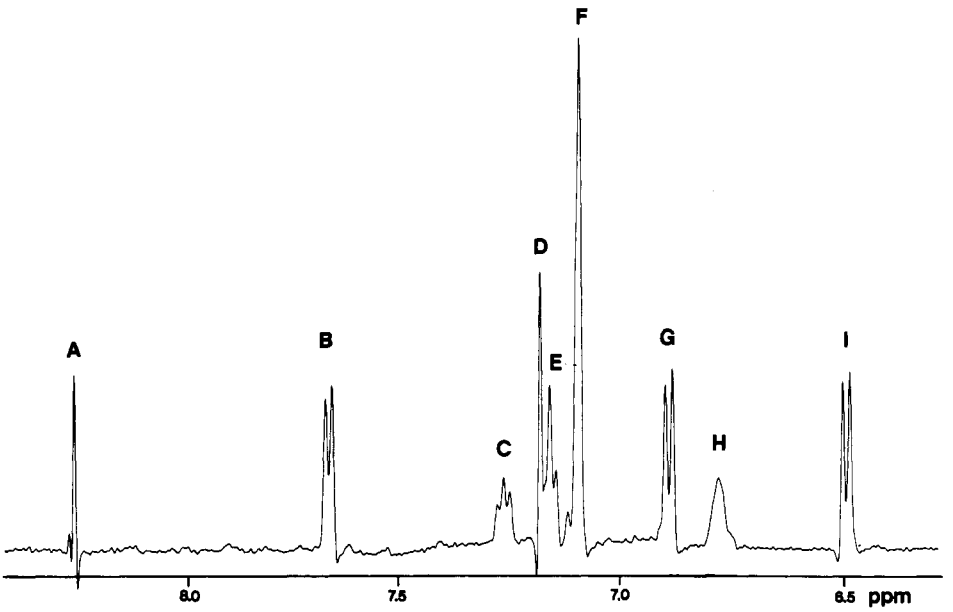

FIGURE 2: Resolution-enhanced spectrum of the downfield aromatic region. Conditions are identical with those in Figure 1. The data have been processed with a Lorentzian to Gaussian transformation to improve resolution.

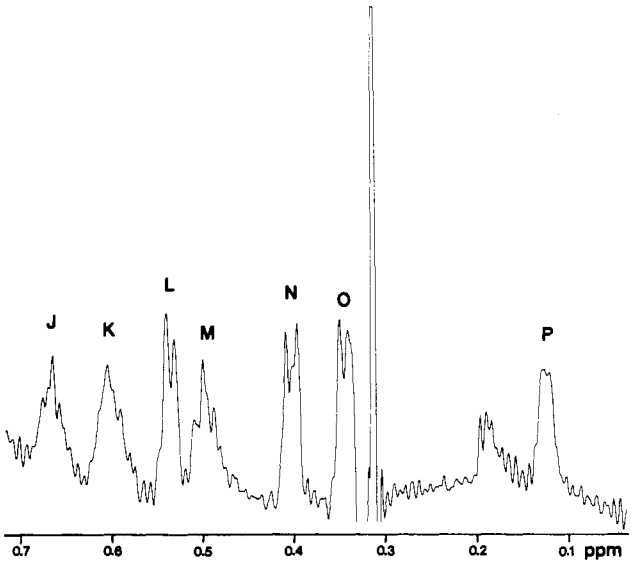

FIGURE 3: Resolution-enhanced spectrum of the upfield ring current shifted resonances. Conditions are the same as in Figure 2.

leucines in the ACP amino acid sequence (Vanaman et al., 1968a,b); only one of these is adjacent to an aromatic residue (Tyr-71–Ile-72) in the sequence. If the other isoleucine triplets are high field shifted due to ring current shift effects, they offer potential structural information. The doublet resonances could correspond to isoleucine, leucine, valine, or threonine γ-methyls which are all spin coupled to one other proton. Through-bond spin–spin coupling correlation and through-space NOE correlations from two-dimensional spectra or one-dimensional experiments offer means of refining assignments. For the resonances of interest here, poorly resolved scalar spin coupling and a very complex methylene region make NOE studies the more reasonable initial choice. Furthermore, NOE experiments provide structural data which, with more refined experiments, can be quantified. NOE difference spectra at 303 K obtained by subtracting spectra with radio frequency (rf) irradiation on and off a resonance of interest for 0.2 s are presented in Figures 4a–c, 5a–c, and 6a–e.

Since the assignments of the Tyr-71 2,6 and 3,5 doublets, peaks G and I, respectively, have been made and the resonances are well resolved (Galley et al., 1978), these provide a logical starting point for NOE analysis. Both of these doublets were irradiated (Figure 4a,b). Irradiation of the Tyr-71 3,5 (I) doublet (Figure 4a) gives NOEs to peaks J and N [an upfield Ile (three-proton) triplet and an upfield Ile (three-proton) doublet, respectively], to the His-75 C(2) proton (A), to its own 2,6 protons (G), and to several other nonassigned upfield resonances. Irradiation of the Tyr-71 2,6 (G) doublet (Figure 4b) again gives an NOE to its own 3,5 protons (I) and peaks K, M, N, and P [two Ile (three-proton) triplets and two (three-proton) doublets, respectively] and a smaller NOE to the His-75 C(2) proton (A), as well as to four other resonances upfield of HDO (i.e., peaks G1, G2, G3, and G4). Intensities at peaks F and H are discounted because of the possibility of direct saturation. Intensities around 1 ppm will not be discussed due to the numerous unresolved aliphatic resonances in this area. The NOE on the 3,5 resonance when irradiating the 2,6 resonance, and vice versa, is not unexpected since 2–3 and 5–6 pairs are only 2.49 Å distant from one another. Observation of NOEs for resonances in the 2–4 ppm region (peaks G1, G2, G3, and G4) is also not unexpected since resonances from the Tyr β-CH_2 and α-CH protons ($\sim$3 Å from the 2,6 protons) could fall here. Peak G1 clearly falls in a region characteristic of aromatic α-CH protons, and peaks G2, G3, and G4 clearly fall in a region characteristic of aromatic β-CH_2 protons (Wagner et al., 1981; Wüthrich et al., 1982; McDonald & Phillips, 1973). The relative amplitudes of peaks G1, G3, and G4 do not vary when sample conditions (i.e., lower temperature or high pH) are varied; peak G2 varies greatly depending on such conditions. Peaks G1, G3, and G4, therefore, are very strongly spacially correlated to the Tyr-71 2,6 protons (G). These peaks are, therefore, tentatively assigned to the Tyr-71 α-CH (G1) and nondegenerate β-CH_2 (peaks G3 and G4) protons.

The NOEs involving isoleucine triplets (J, K, and M) provide desired assignment and structural information. The NOE of one of the isoleucine triplets is expected due to a proximity relationship in the sequence between Tyr-71 and Ile-72 and can provide a tentative assignment of either peak J, peak K, or peak M to the δ-methyl of Ile-72. The NOE of a second and third upfield Ile triplet is unexpected and provides additional pieces of structural information, namely,

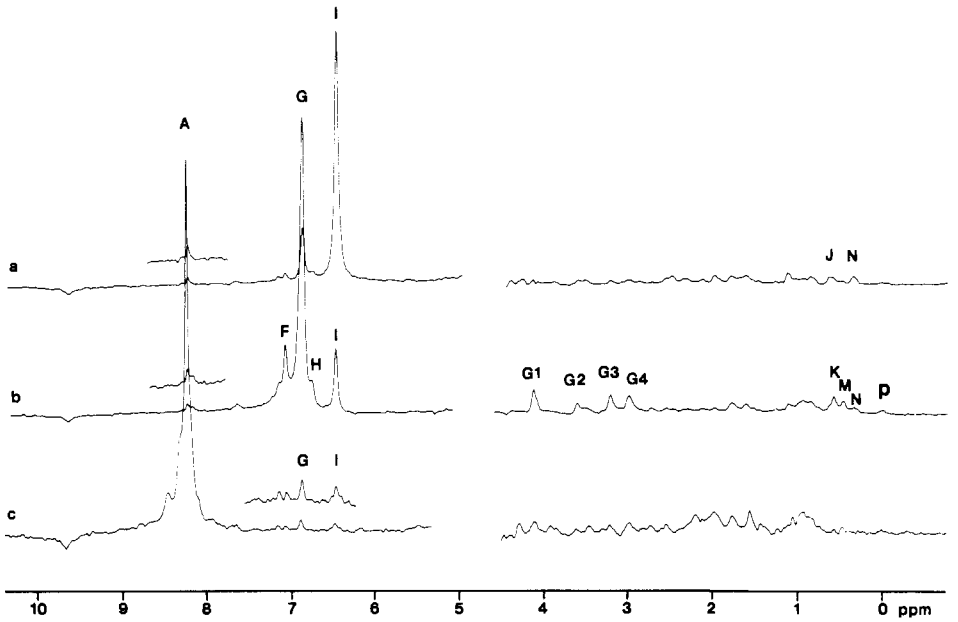

FIGURE 4: NOEs given by ACP-SH. Three NOE difference spectra are shown, each representing the difference between an accumulation of 1500 FIDs taken with saturating rf off-resonance and another accumulation of 1500 FIDs taken with saturating rf on-resonance. In each case, the rf saturation time was 0.2 s. Spectra are for saturation of resonance I (a), resonance G (b), and resonance A (c). Labeling of resonances is as in Figure 1 and as described in the text.

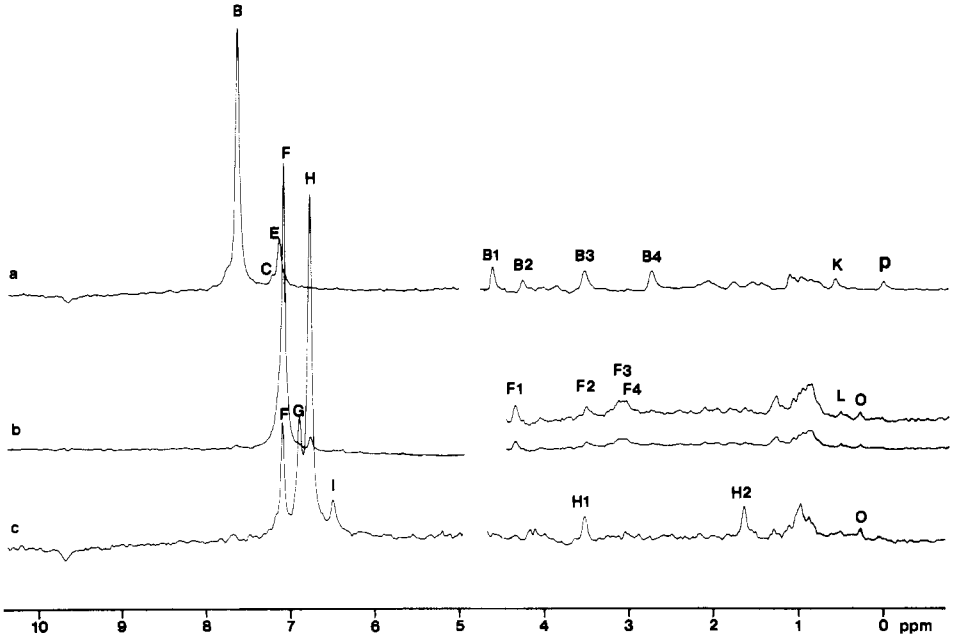

FIGURE 5: NOEs given by ACP-SH. Three NOE difference spectra are shown with accumulation as described in Figure 4. Spectra are for saturation of resonance B (a), resonance F (b), and resonance H (c).

that a second isoleucine and a third isoleucine are in the vicinity of Tyr-71. It is possible that the doublets (N and P) arise from the γ-methyl protons on two of the isoleucines.

A further piece of structural information is found in the unexpected NOE between the Tyr-71 2,6 and 3,5 protons and the His-75 C(2) proton (A). Irradiation of peak A, the His-75 C(2) proton, shows small NOEs to both Tyr-71 2,6 and 3,5 proton resonances (Figure 4c), confirming the connectivity shown in experiments whose results are displayed in Figure 4a,b. Although amplitudes are small, the data are strengthened by the fact that these NOEs become larger at lower temperatures.

Irradiation of peak B, the Phe-I 2,6 protons (Figure 5a), in an NOE experiment clearly perturbs its own 3,5 (peak E) and 4 (peak C) proton resonances, peak K (one of the Ile-upfield triplets), and peak P (one of the upfield doublets), as well as four other upfield resonances, peaks B1, B2, B3, and B4. Peaks B1 and B2 fall in a region typical for aromatic residue α-CH protons, and peaks B3 and B4 fall in a region typical for aromatic β-CH_2 protons. Again as was the case for the Tyr-71 β-CH_2 assignments, peaks B1, B3, and B4 do not vary in relative amplitude as a function of changing environmental conditions. Peak B2 varies significantly in amplitude under varying conditions and cannot be as strongly spacially correlated to the Phe-I 2,6 protons (B) as can peaks B1, B3, and B4. Tentative assignments can be made for the Phe-I α-CH (B1) and the nondegenerate Phe-I β-CH_2 (peaks B3 and B4) protons. Peaks K and P also demonstrate through-space connectivities to Tyr-71, strongly suggesting Phe-I and Tyr-71 are not too distant from one another—a further piece of interesting structural information. Irradiation of peaks E and C, which are also assigned to phenylalanine-I,

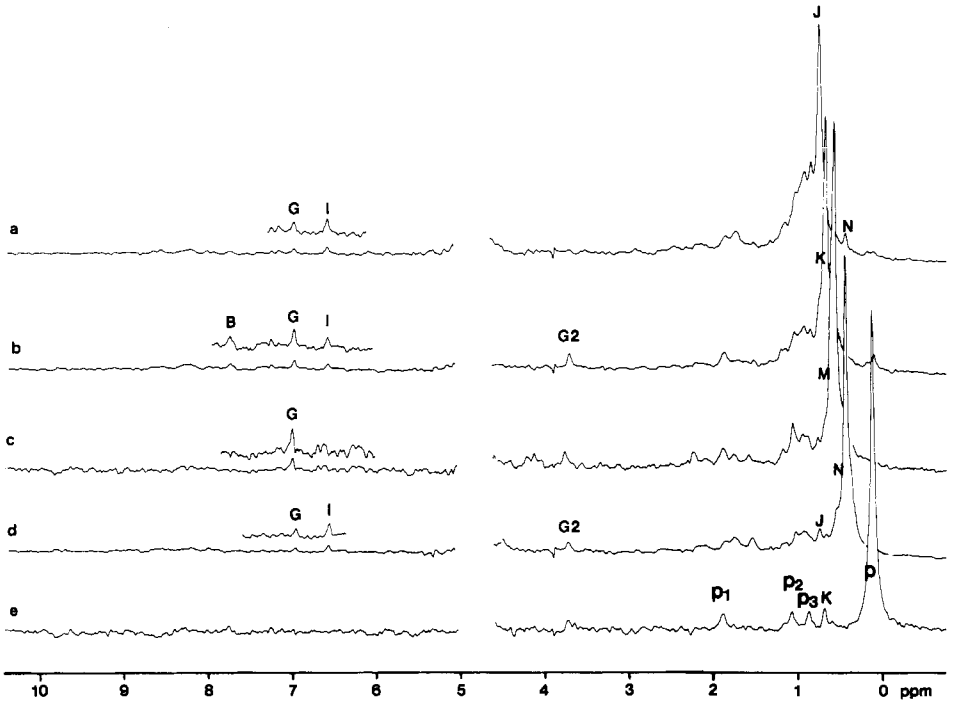

FIGURE 6: NOEs given by ACP-SH. Five NOE difference spectra are shown with accumulation as described in Figure 4. Spectra are for saturation of resonance J (a), resonance K (b), resonance M (c), resonance N (d), and resonance P (e).

will not be considered because of difficulties in resolving these resonances from the His-75 C(4) proton resonance.

Irradiation of the Phe-II 2,6 + 3,5 protons (peak F) (Figure 5b) perturbs peak H, the Phe-II 4 proton. Two upfield ring current shifted doublet resonances (peaks L and O) clearly show NOEs from peak F; these doublet resonances of intensity 3 (peaks L and O) most likely belong to γ-methyl groups of isoleucine, leucine, valine, or threonine residues. Four well-resolved resonances in the NOE difference spectrum (Figure 5b) are also seen slightly upfield of HDO (peaks F1, F2, F3, and F4). Using similar arguments as were employed in the NOE results for both Tyr-71 and Phe-I, we can say that F1 exists in an aromatic α-CH region, and peaks F2, F3, and F4 exist in an aromatic β-CH_2 region (Wagner et al., 1981; Wüthrich et al., 1982). Peak F2 varies significantly relative to peak H as a function of environmental conditions, whereas peaks F1, F3, and F4 do not; therefore, tentative assignments of peaks F1, F3, and F4 can be made to the Phe-II α-CH and nondegenerate β-CH_2 protons, respectively.

Irradiation of peak H, the Phe-II 4 proton (Figure 5c), perturbs peaks H1, H2, and O, an upfield ring current shifted doublet, as well as the expected perturbation of peak F, the Phe-II 2,6 + 3,5 protons. Peak H1 is, more likely than not, equatable with peak F2 since they appear at 3.52 ppm and arise from irradiation of protons on the same phenylalanine-II residue, rendering further credence to our assignments of peaks F1, F3, and F4 as discussed above. The fact that irradiation of peak H perturbs peak F2, as did irradiation of F, indicates that peak F2 is, more likely than not, neither the α-CH nor the β-CH_2 Phe-II protons which should only show NOEs to the 2,6 ring protons. Irradiation of either of these Phe-II peaks (i.e., F or H) produces no readily interpretable structural information. NOEs to peaks G and I will be dismissed due to the possibility of direct saturation to peak G and/or to peak I.

Suggestions of structural and assignment information, made on the basis of irradiation of aromatic resonances, can be confirmed by performing the inverse experiments in which ring current shifted, high-field resonances are irradiated, and NOEs on other resonances are observed; again, the investigation is confined to well-resolved resonances.

Peaks K and M, assigned to isoleucine δ-methyls, were suggested to interact with protons on Tyr-71, and peak K was suggested to interact with the 2,6 protons on Phe-I. Irradiation of peak J (Figure 6a) also produces an NOE at the Tyr-71 2,6 and 3,5 doublets. Figure 6b demonstrates that irradiation of peak K produces the expected NOEs at the Tyr-71 2,6 (G) and 3,5 (I) protons and at the Phe-I 2,6 (B) doublets. Irradiation of peak M (Figure 6c), the third upfield ring current shifted isoleucine δ-methyl resonance, clearly perturbs the Tyr-71 2,6 protons (G). This confirms the presence of three isoleucines near Tyr-71.

Irradiation of peak J or K also shows NOEs to one further upfield ring current shifted doublet each, peaks N and P, respectively. When peaks N and P are irradiated themselves (spectra d and e, respectively, of Figure 6), they give NOEs back to the respective δ-methyl groups (peaks J and K). Of the possible conformations in the isoleucine side chain, one where rotation about the C_β–C_γ-methylene bond places the γ- and δ-methyl groups of the same residue in close proximity to each other (2–3 Å) could account for the observed NOEs between these upfield doublets (N and P) and triplets (J and K). On this basis, we group peaks J and N and peaks K and P as belonging to the δ- and γ-methyl resonances, respectively, of the same isoleucine residues (i.e., Ile-I for the J, N pair and Ile-II for the K, P pair). As indicated in Figure 6d, irradiation of peak N also shows a clear NOE on the Tyr-71 2,6 (G) and 3,5 (I) proton resonances, confirming the proximity of the Tyr-71 and Ile-I.

Irradiation of the upfield Ile-II γ-methyl doublet (P) (Figure 6e), aside from demonstrating the expected reciprocal NOE on the Ile-II δ-methyl triplet (K), produces an additional four rather distinct NOEs—one to peak G2, also perturbed by irradiation of the Tyr-71 2,6 protons (G), and three others (i.e., peaks P1, P2, and P3) in regions appropriate for resonances arising from other protons on the isoleucine side chain (i.e., the β-CH and two, nondegenerate γ-CH_2 protons); specific assignments at this time are impossible.

Table I: Resonance Assignments

peak	assignment	chemical shift (ppm)
Upfield Ring Current Shifted Resonances (Aliphatic Side Chain)		
J	Ile-I δ-CH_3	0.66
K	Ile-II δ-CH_3	0.60
N	Ile-I γ-CH_3	0.40
P	Ile-II γ-CH_3	0.12
L	Leu, Ile, Thr, or Val δ-CH_3	0.53
M	Ile-III δ-CH_3	0.50
O	Leu, Ile, Thr, or Val δ-CH_3	0.34
α-CH, β-CH_2, and Other Aliphatic Residue Resonances		
B1	Phe-28 α-CH	4.62
B2	(?)	4.26
B3	Phe-28 β-CH	3.55
B4	Phe-28 β-CH	2.74
F1	Phe-50 α-CH	4.35
F2	(?)	3.52
F3	Phe-50 β-CH	3.14
F4	Phe-50 β-CH	3.04
G1	Tyr-71 α-CH	4.18
G2	(?)	3.66
G3	Tyr-71 β-CH	3.30
G4	Tyr-71 β-CH	3.08
P1	Ile-II β-CH	1.83
P2	Ile-II γ-CH	1.01
P3	Ile-II γ-CH	0.80
Aromatic Region		
A	His-75 C(2)	8.27
D	His-75 C(4)	7.19
B	Phe-28 2,6	7.65
C	Phe-28 4	7.23
E	Phe-28 3,5	7.17
F	Phe-50 2,6 and 3,5	7.08
H	Phe-50 4	6.78
G	Tyr-71 2,6	6.89
I	Tyr-71 3,5	6.49

Irradiation of peaks potentially identified as aromatic β-CH_2 proton resonances produces expected NOE enhancement of aromatic region resonances. NOEs to other regions of the spectrum are also noted, and tentative assignment of resonances of other proximal residues can be made. Due to spectral overlap of several resonances in this region, there is a level of ambiguity introduced that makes reliance on these assignments for structural data unadvisable.

In summary, some tentative assignments of resonances in the upfield region of the NMR spectrum (Figure 1) can be made. Specifically, peaks J and N belong to the δ- and γ-methyl groups, respectively, on one isoleucine (Ile-I); peaks K and P belong to the δ- and γ-methyl groups, respectively, on another isoleucine (Ile-II), and peak M belongs to a δ-methyl group on a third isoleucine residue (Ile-III), all three isoleucines being conformed in the vicinity of Tyr-71. One of these three isoleucines is very likely Ile-72; the next nearest isoleucine in the primary amino acid sequence is Ile-69. The Tyr-71 α-CH and β-CH_2 resonances have been assigned, as well as the α-CH and β-CH_2 resonances for Phe-I and Phe-II, which have been labeled as Phe-28 and -50, respectively, and will be justified later in the discussion in terms of the probable structure. These resonance assignments are given in Table I. We have also uncovered some interesting structural data, namely, that an isoleucine close to Tyr-71 is also close to Phe-28 and that Tyr-71 is proximal to His-75.

Nuclear Overhauser Effects: Quantitative Results. In ideal situations, proximity relationships can be made more quantitative by consideration of the time dependence of the NOEs, and we will attempt to achieve this for some of the relationships we have discussed. For a system of dipolar coupled spins, the magnitude of the nuclear Overhauser effect on a given spin following saturation of another spin for a fixed length of time depends on the motional properties of the spin system, on the resonance frequency of the spectrometer, and, for our immediate interest in this section, on the inverse sixth power of the distances separating pairs of spins; therefore, nuclear Overhauser effects contain much information about structural and dynamical properties (Sykes et al., 1974; Oldfield et al., 1975; Chapman et al., 1978; Kirshna et al., 1978; Gordon & Wüthrich, 1978; Poulsen et al., 1980). An analysis of any such effects can be quite complex as a rigorous treatment requires consideration of a highly coupled set of cross-relaxation interactions as well as a detailed model for molecular motion (Bothner-By & Noggle, 1979; Wagner & Wüthrich, 1979; Trapp, 1980).

Dobson et al. (1980) and Poulson et al. (1980) have recently shown that relative nuclear Overhauser effects measured shortly after saturation of assigned resonances in the proton NMR spectrum of a large protein, lysozyme, at high field (498 MHz) can be directly correlated with the inverse sixth powers of interproton distances taken from the crystal structure. The treatment is based on the fact that for short times, direct cross-relaxation between pairs of protons dominates the establishment of NOEs, and formulas for a two-spin system, in which effects of other spins are included only as random field relaxation, apply reasonably well.

For a two-spin system, the full time dependence of the nuclear Overhauser effect is given by eq 1 (Noggle & Shirmer,

$$\eta_j(t) = (\sigma_{ij}/\rho_j)(1 - e^{-\rho_j t}) \quad (1)$$

1971) where $\eta_j(t)$ is the nuclear Overhauser effect, σ_{ij} is the cross-relaxation rate between protons i (the irradiated proton) and j, and ρ_j is the direct relaxation rate of proton j. When this is applied to multispin systems, ρ_j includes all relaxation contributions. Failure of this treatment can be seen as a departure from exponential buildup, often with later time points enhanced by indirect pathways (spin diffusion). Panels a, b, and c of Figure 7 present plots of $\eta_j(t)$ vs. the saturation (development) time, t, for resonances observed on irradiating the Tyr-71 2,6 and 3,5 protons and the Phe-I 2,6 proton resonances, respectively, at 303 K. Most of these plots are consistent with exponential growth having monotonically decreasing rates of growth as time is increased. A few plots deviate, however, from this behavior and increase their rates of growth at intermediate times. For example, the development of an NOE for the His-75 C(2) proton resonance (A) (Figure 7a) demonstrates such a departure from exponential buildup at 0.4 s when observed by irradiating the Tyr-71 2,6 proton resonance; when, however, the Tyr-71 3,5 proton resonance is irradiated, there is no such anomaly, suggesting that indirect mechanisms contribute to the NOE beyond 0.2 s for 2,6 irradiation. This is inconsequential for our qualitative arguments placing one residue in the neighborhood of another, but it does indicate that the NOE for the His-75 C(2) proton resonance on Tyr-71 2,6 irradiation should not be used in quantitative distance interpretations.

For the remaining data, σ_{ij} and ρ_j can be extracted by an iterative direct search fit of eq 1. ρ_j can be estimated from first-order kinetic plots of log $[1 - \eta_j(t)/[\eta_j(\infty)]]$ vs. the saturation time (t); σ_{ij} can be estimated from the initial slopes in Figure 7a–c or by using the estimated ρ_j value with eq 1 and calculating a σ_{ij} value. These estimates for σ_{ij} and ρ_j were used as initial points in the direct search. These results are summarized in Table II. The cross-relaxation terms (σ_{ij}) can be written as a product of a term dependent on $1/(r_{ij})^6$, where r_{ij} is an internuclear distance, and a spectral density function

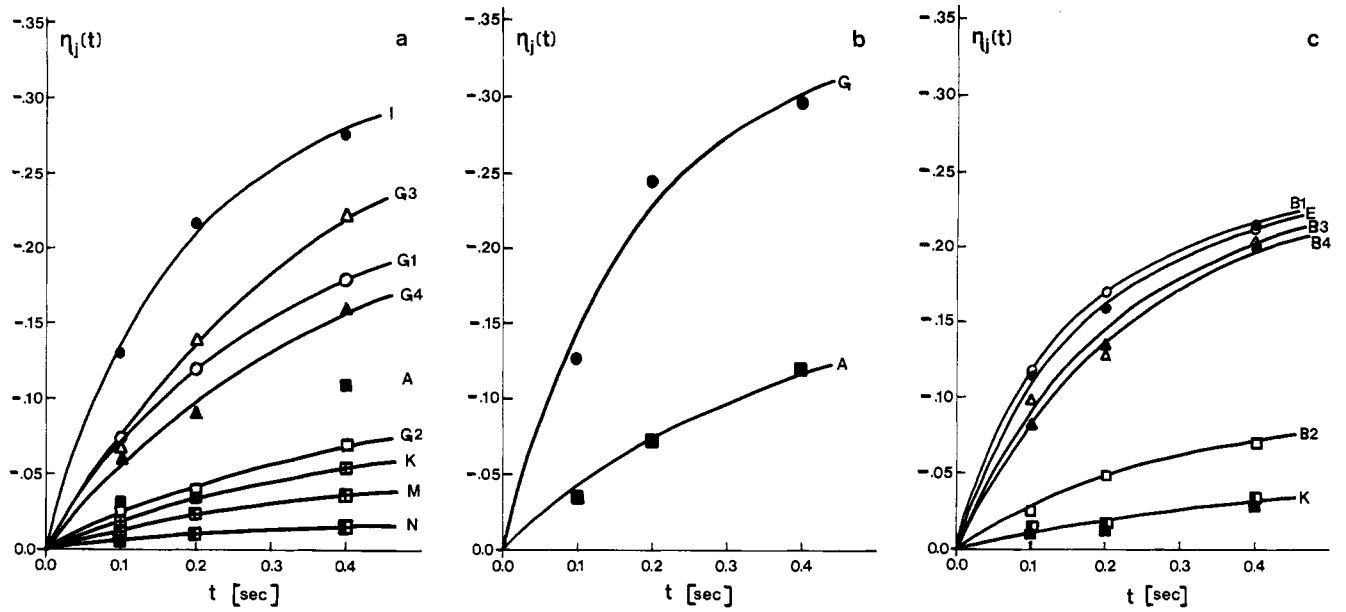

FIGURE 7: Percent NOE vs. saturation time. Three graphs showing the time dependence of the development of NOEs from aromatic resonances are shown. Irradiation of resonance G (a); irradiation of resonance I (b); irradiation of resonance B (c). Acquisition is as described in Figure 4, except that the saturation time is varied. The experimental points are shown as labeled in the figures. Direct search fits of eq 1 to the experimental data are shown as solid lines.

Table II: Cross-Relaxation Rates and Internuclear Distances

irradiated proton(s)	peak showing NOE	σ_{ij} (s^{-1}) (T = 303 K)	σ_{ij} (s^{-1}) (T = 288 K)	$\sigma_{ij(303)}/\sigma_{ij(288)}$	r_{ij} (Å)
Phe-28 2,6	Phe-28 3,5	−1.47	−2.6	0.6	2.49[a]
	Phe-28 α-CH	−1.65	−2.8	0.6	2.4
	B2	−0.32[b]	−0.45[b]	0.7	(3.2)[b]
	Phe-28 β-CH	−1.04	−1.46	0.7	2.6
	Phe-28 β-CH	−0.97	−1.37	0.7	2.7
	(K) Ile-II δ-CH_3	−0.12	−0.37	0.3	(3.8)
	(P) Ile-II γ-CH_3	−0.11	−0.28	0.4	(3.8)
Tyr-71 2,6	Tyr-71 3,5	−1.79	−3.1	0.6	2.49[a]
	Tyr-71 α-CH	−0.83	−1.31	0.6	2.8
	G2	−0.29[b]	−0.4[b]	0.7	(3.4)[b]
	Tyr-71 β-CH	−0.74	−1.08	0.7	2.9
	Tyr-71 β-CH	−0.58	−0.84	0.7	3.0
	His-75 C(2)		spin diffusion		
	(K) Ile-II δ-CH_3	−0.21	−0.46	0.5	(3.6)
	(P) Ile-II γ-CH_3		spin diffusion		
	(M) Ile-III δ-CH_3	−0.15			(3.8)
	(N) Ile-I δ-CH_3	−0.13			(3.9)
Tyr-71 3,5	Tyr-71 2,6	−1.88	−2.75	0.7	2.49[a]
	His-72 C(2)	−0.37	spin diffusion		(3.3)

[a] Values used as calibration of internuclear distances. [b] Estimates of values where number of protons is not known; calculated with the assumption of their being two protons.

dependent on τ_c, an effective correlation time for internuclear vector reorientation. In cases where τ_c can be considered the same for all residues, two measurements of σ_{ij} can give relative distances.

The possibility of different interactions having different correlation times is a problem which is more difficult to detect than indirect pathway contributions to nonexponential growth of NOEs. It is a potential problem for groups such as isoleucine where internal bond isomerizations could make important contributions to τ_c. One possible way to explore τ_c is indirectly via temperature. If two interactions are modulated by the same motions and the r_{ij} values do not change as a function of temperature, then the σ_{ij} values should have the same temperature dependence. σ_{ij} values determined at both 288 and 303 K are therefore presented in Table II. Their ratios are the same for many residues; those residues whose ratios are not the same should be excluded from more quantitative consideration. This deviation in the ratios of the σ_{ij} values is governed either by a different τ_c or by conformational changes as a function of temperature.

Distances calculated by using the known Tyr-71 2,6 to 3,5 or Phe 2,6 to 3,5 proton distances (i.e., 2.49 Å) as a reference are given in the last column of Table II. Distances have been calculated even in cases where there is reason to question quantitative reliability because of different temperature dependencies of σ_{ij} or the contribution of indirect pathways at long times. These distances are in parentheses. In other cases, distances should be more quantitatively reliable.

Discussion

The tentative assignments and the through-space connectivities as detected by NOE measurements provide a stringent test for proposed structural models of ACP. Ideally, highly accurate interresidue distances calculated from NOEs can be compared to distances measured in various conformational models. Unfortunately, as can be seen in Table II, our most

reliable distances involving assigned resonances are intra- rather than interresidue. Most intraresidue distances are, in fact, very reasonable and provide additional confirmation of assignments. For example, 2.6–3.0 Å is well within the range expected for aromatic 2,6 proton to β-CH_2 proton distances.

Interresidue distances, while less reliable, offer considerable insight into models for tertiary folding even if error limits on the order of 1 Å are applied to the numbers given in parentheses. The most detailed model to date is that proposed by Rock & Cronan (1979) on the basis of the Chou–Fasman predictive algorithm. While this model applies only to the secondary structure, namely, the four predicted α-helical segments, it will provide a starting point for our discussion. Our data lend support for the strongly predicted α-helical segments in the sense that reasonable models can be found without redefining these α-helical segments. In addition, there is some direct support for the secondary structure near the C terminus.

On the basis of our NOE data, three isoleucine residues (i.e., Ile-I, -II, and -III) and Tyr-71 lie close to one another in the dominant ACP solution structure. Quantitative evaluation of distances is difficult because of internal motions in these groups. Distances given in Table II can, however, be taken as a rough guideline (i.e., 3–4-Å separation between the isoleucine δ- and γ-methyl groups and the Tyr-71 2,6 and 3,5 protons). Ile-69, Ile-72, and Tyr-71 are all close to one another near the C terminus of the amino acid sequence, but not all conformations of the C terminus segment allow distances of approach within the ranges suggested above; a proposal, which would permit the α-helical segment 4 (residues 58–69) to include both Ile-69 and Ile-72, would, for example, place Ile-69 on the side of the α-helix opposite that of Tyr-71, physically removing the possibility of an NOE between Ile-69 and Tyr-71. The secondary structure of ACP-SH, proposed from the Chou–Fasman algorithm (Rock & Cronan, 1979), indicates that residues 70–72 have a high probability of being in a β-sheet conformation, but were predicted as random coil because the section of the protein running from Asp-70 to the C-terminus end was considered too short to participate in β-sheet nucleation. Beginning a β-bend at the Tyr-71 C_α-NH bond and continuing with a more extended sequence place each of two Ile residues (Ile-69 and -72) on each side of Tyr-71, sandwiching Tyr-71 between them. A reasonable population of such a conformer explains the observed NOEs. Two of these three isoleucine residues (i.e., Ile-I, -II, and -III) are then assignable to Ile-69 and -72.

Further out on the C terminus we find His-75. NOE data (Table II) suggest that the C(2) proton of His-75 and the 3,5 protons of Tyr-71 are approximately 3 Å apart in the tertiary structure of ACP-SH. The data therefore require that this terminal segment somehow folds back on itself. If we fold the segment by using α-helical geometry, in other words, extend the C-terminal α-helical segment (amino acid residues 57–69) to include the entire C terminus, it is possible to bring His-75 and Tyr-71 into close proximity with one another; doing this would, however, destroy the isoleucine-69 and -72 contacts with Tyr-71 described above. A second β-turn at Gly-74 is predicted with high probability (Rock & Cronan, 1979); such a β-turn at this point in the sequence would reverse the chain direction at residue 74, allowing both the His-75 C(2)–Tyr-71 3,5 proton contact and the Ile-69–Tyr-71–Ile-72 contacts. Thus, there is reasonable support for some proposed secondary structural features of the C terminus.

The Chou–Fasman predictive model (Rock & Cronan, 1979) provides no information concerning the folding of the various α-helical segments into a three-dimensional (tertiary) structure. The NOE data placing Tyr-71, Ile-I, -II, and -III, and a phenylalanine in close proximity put stringent limitations on protein folding. The data demonstrating through-space interactions among the Ile-II δ- and γ-methyls, represented by peaks K and P, respectively, and the Phe-I 2,6 protons provide one vital piece of structural information. Phe-I is suggested to be within ~4 Å of the Ile-II K and P peaks. Two phenylalanines are present in ACP, Phe-28 and -50 (Vanaman et al., 1968a,b). In the Chou–Fasman predictive model, Phe-50 is near the carbonyl end of α-helix 3 (amino acid residues 38–53), and the isoleucines are near Tyr-71 at the carbonyl end of α-helix 4 (amino acid residues 57–69). If the general features of the predictive model are correct, it is improbable that Phe-50 could be brought near Tyr-71 even if α-helix 4 were to fold back directly on α-helix 3. A high probability exists, however, that Phe-28, positioned in the middle of the short α-helical segment 2 (amino acid residues 26–32), could be positioned into close proximity with the C-terminal random-coil region by folding α-helical segments 1–4 back on one another as depicted in Figure 8. Phe-I is, therefore, equated with Phe-28, and, by deduction, Phe-II with Phe-50.

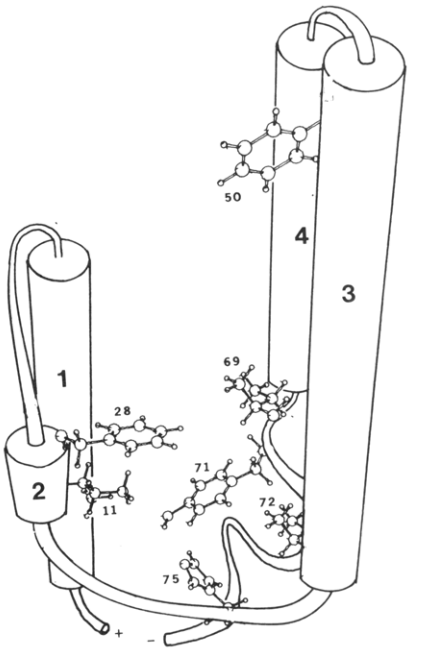

FIGURE 8: Proposed tertiary structure of ACP-SH. The proposed gross conformation of ACP-SH is shown. α-Helix regions (1–4) are depicted as cylinders and are labeled as described in the text; β-turns and random coils are shown as solid lines. The only amino acid residues shown are those for which NOE data have been presented.

The presence of an NOE between Tyr-71 and the δ-methyl group of a third isoleucine residue (Ile-III) adds still one further important piece of tertiary structural information as to how the various proposed α-helical chains are folded. As mentioned above, two of the seven isoleucines present in *E. coli* ACP (Vanaman et al., 1968a,b) (Ile-69 and Ile-72) lie in a linear sequence close to Tyr-71. Of the remaining five isoleucines (Ile-3, -10, -11, -54, and -62), two of them (Ile-54 and -62) are located at, or closer to, the N-terminal end of the C-terminus α-helical segment (residues 58–69), and if we accept the general features of the predictive model, the possibility of contact between Tyr-71 and either Ile-54 or Ile-62 is physically removed. The only remaining option of bringing a third isoleucine δ-methyl group to within 3–4 Å of Tyr-71 is to bring the N-terminus α-helical segment 1 (residues 3–21),

where all three of the remaining possible isoleucine residues are located anyway (i.e., Ile-3, -10, and -11), into contact with the C-terminus α-helical segment 4 (residues 58–69) as depicted in Figure 8.

The folding suggested above, with α-helix 2, containing Phe-28, and α-helix 1 (N terminus) being adjacent to α-helix 4 (C terminus), places most of the molecule's hydrophobic residues at the interior of the protein molecule and most of the hydrophilic residues at the surface of the protein. The prosthetic group lies in a central hydrophobic corridor of the protein in which all four aromatic residues are arranged in an almost linear array. A hydrophobic interior and a hydrophilic exterior (surface) present the usual picture of a protein molecule in aqueous solution. Looking at the tertiary model in Figure 8, one can imagine that the positively charged His-75 could form a salt bridge with the diesterified phosphate of the prosthetic group, and the negatively charged carboxyl group of the C-terminus terminal residue (Ala-77) could form a salt bridge with the NH-terminal residue (Ser-1) to essentially anchor both the C and NH termini. It should also be mentioned, in conclusion, that the folding of the four α-helix chains in this way (Figure 8) not only allows for a hydrophobic pocket (corridor) to be present in ACP for the binding of the prosthetic group and acyl chain, but also such folding allows for the thio ester bond and the C(2)–C(3) carbon bond of a bound acyl chain to be in a site accessible to enzymes of the fatty acid synthetase system from that side of the ACP molecule where the α-helical 2 and 3 segments are folded onto one another. It is at this C(1)–C(3) segment of the growing acyl chain where most of the chemistry of chain elongation, reduction, and dehydration occurs in conjunction with the enzymes of the fatty acid synthetase system.

A more exact functional nature of these secondary and tertiary structural interactions is, at present, impossible to evaluate. The fact that interhelix NOEs exist, however, provides a powerful tool to examine conformational changes induced in ACP as a function of changes in pH, ionic strength, or other added effector molecules. Both pH and ionic strength have been previously suggested to affect the structure of ACP profoundly and, in fact, may be involved in modulation of enzymatic activities of the fatty acid synthetase system (Schultz et al., 1969; Schultz, 1975).

Acknowledgments

We thank Neel Scarsdale for producing the ORTEP drawing of the proposed ACP structure.

Registry No. Tyr, 60-18-4; Ile, 73-32-5; His, 71-00-1; Phe, 63-91-2.

References

Bothner-By, A. A., & Noggle, J. H. (1979) *J. Am. Chem. Soc. 101*, 5152–5156.

Chapman, G. E., Abercrombie, B. D., Cary, P. D., & Bradbury, E. M. (1978) *J. Magn. Reson. 31*, 459–468.

Chou, P. Y., & Fasman, G. D. (1974a) *Biochemistry 13*, 211–221.

Chou, P. Y., & Fasman, G. D. (1974b) *Biochemistry 13*, 222–245.

Chou, P. Y., & Fasman, G. D. (1978a) *Annu. Rev. Biochem. 47*, 251–276.

Chou, P. Y., & Fasman, G. D. (1978b) *Adv. Enzymol. Relat. Areas Mol. Biol. 48*, 45–148.

Cronan, J. E., Jr., & Klages, A. L. (1981) *Proc. Natl. Acad. Sci. U.S.A. 78*, 5440–5444.

Dobson, C. M., Hoch, H. C., Olejniczak, E. T., & Poulsen, F. M. (1980) *Biophys. J. 32*, 625–636.

Ellman, G. L. (1959) *Arch. Biochem. Biophys. 82*, 70–77.

Galley, H. U., Spencer, A. K., Armitage, I. M., Prestegard, J. H., & Cronan, J. E., Jr. (1978) *Biochemistry 17*, 5377–5382.

Gordon, S., & Wüthrich, K. (1978) *J. Am. Chem. Soc. 100*, 7094–7098.

Krishna, N. R., Agresti, D. G., Glickson, J. D., & Walter, R. (1978) *Biophys. J. 24*, 791–802.

McDonald, C. C., & Phillips, W. D. (1973) *Biochemistry 12*, 3170–3186.

Noggle, J. H., & Shirmer, R. E. (1971) *The Nuclear Overhauser Effect*, Academic Press, New York.

Oldfield, E., Norton, R. S., & Allerhand, A. (1975) *J. Biol. Chem. 250*, 6368–6375.

Poulsen, F. M., Hoch, J. C., & Dobson, C. M. (1980) *Biochemistry 19*, 2597–2601.

Prescott, D. J., & Vagelos, P. R. (1972) *Adv. Enzymol. Relat. Areas Mol. Biol. 36*, 269–311.

Prescott, D. J., Elovson, J., & Vagelos, P. R. (1969) *J. Biol. Chem. 244*, 4517–4521.

Ray, T. K., & Cronan, J. E., Jr. (1976) *Proc. Natl. Acad. Sci. U.S.A. 73*, 4374–4378.

Rock, C. O., & Cronan, J. E., Jr. (1979) *J. Biol. Chem. 254*, 9778–9785.

Rock, C. O., & Cronan, J. E., Jr. (1980) *Anal. Biochem. 102*, 362–364.

Schultz, H. (1975) *J. Biol. Chem. 250*, 2299–2304.

Schultz, H., Weeks, G., Toomey, R. E., Shapiro, M., & Wakil, S. J. (1969) *J. Biol. Chem. 244*, 6577–6583.

Sykes, B. D., Weingarten, H. I., & Schlesinger, M. J. (1974) *Proc. Natl. Acad. Sci. U.S.A. 71*, 469–474.

Takagi, T., & Tanford, C. (1968) *J. Biol. Chem. 243*, 6432–6435.

Thompson, G. A. (1981) *The Regulation of Membrane Lipid Metabolism*, pp 20–23 and 33, CRC Press, Boca Raton, FL.

Trapp, J. (1980) *J. Chem. Phys. 72*, 6035–6041.

Vanaman, T. C., Wakil, S. J., & Hill, R. L. (1968a) *J. Biol. Chem. 243*, 6409–6419.

Vanaman, T. C., Wakil, S. J., & Hill, R. L. (1968b) *J. Biol. Chem. 243*, 6420–6431.

Wagner, G., & Wüthrich, K. (1979) *J. Magn. Reson. 33*, 675–687.

Wagner, G., Kumar, A., & Wüthrich, K. (1981) *Eur. J. Biochem. 114*, 375–384.

Wüthrich, K., Wider, G., Wagner, G., & Braun, W. (1982) *J. Mol. Biol. 152*, 311–320.